Atomic Arrangements inside Ru and Os Nanoislands Spontaneously Deposited on Pt(111)

Bonseong Ku, Changhoon Jung, and Choong Kyun Rhee*

Department of Chemistry, Chungnam National University, Daejeon, 305-764, Korea

Received: April 6, 2006; In Final Form: May 17, 2006

The atomic arrangements inside Ru and Os nanoislands spontaneously deposited on Pt(111) electrode surface were observed with electrochemical scanning tunneling microscopy. The surperlattice of the pristine Ru nanodeposits is $(\sqrt{3}\times\sqrt{3})R30°$-$RuO^+$. Upon reduction, the Ru nanodeposits are compressed to a uniaxially incommensurate $(\sqrt{3}\times\sqrt{2})R30°$-Ru structure, which does not change during the following reoxidation. The atomic arrangement inside the pristine Os nanodeposits is an incommensurate $(\sqrt{2}\times\sqrt{2})$-OsO^+ structure, which does not transform during the subsequent reduction−oxidation cycles. The structures of the Ru and Os nanodeposits are discussed in terms of removal and insertion of oxygen ions depending on electrode potential.

Introduction

In developing electrocatalysts for the anode of a direct methanol fuel cell, Ru is an important ingredient as a catalytic promoter to Pt base catalysts.[1−10] In addition to Ru, other elements, such as Os and Ir, have been reported to boost the binary catalysts of Pt/Ru toward methanol oxidation.[9,11,12] Surface modification of Pt base catalysts was performed by alloying,[2−4,6−8,11−13] electrochemical deposition,[14−16] vacuum evaporation,[6] and spontaneous adsorption.[5,9,17−19]

In an effort to understand the roles of the catalytic promoters, various attempts have been tried. The catalytic activity of Ru-modified Pt electrodes in methanol oxidation is enhanced by lowering the oxidation potential of CO by ∼150 mV.[20] Such a cathodic shift is understood in terms of a bifunctional effect of Ru.[4,11,21] To deepen the knowledge of the roles of catalytic promoters, the oxidation states of Ru and Os, spontaneously deposited on Pt(111), were investigated with ex situ X-ray photoelectron spectroscopy (XPS) by Wieckowski's group.[18,22] Correlation of the observed oxidation states of the promoters with the methanol oxidation potential reveals that the oxidation current is maximized at the potential in which the metallic state and a certain oxidized state of Ru and Os coexist. On the other hand, structural studies using electrochemical scanning tunneling microscopy (EC-STM) disclosed that the promoter deposits on Pt(111) are nanoislands of 2−5 nm in diameter and are distributed randomly without any local preferences.[17,23] In particular, it is remarkable that an electrochemical treatment of Ru deposits on Pt(111) results in a shrinkage of the deposits both in height and in width, accompanied by an increase in methanol oxidation rates.[19] However, the atomic arrangements of the Ru and Os promoters, which would be critical to understand the role of the promoter at a molecular level, have not yet been revealed.

Presented are the atomic arrangements inside the Ru and Os nanoislands spontaneously deposited on Pt(111). The main focus of this work is the change of the atomic structures inside the islands of Ru and Os, depending on electrode potential.

* Corresponding author. Telephone: 82-42-821-5483. Fax: 82-42-821-8896. E-mail: ckrhee@cnu.ac.kr.

Experimental Section

The Pt(111) single crystals used in this work were obtained by melting a Pt wire (0.5 mm diameter, Aldrich, 99.99%) to a single-crystal bead in a hydrogen−oxygen flame. For voltammetric works, a (111) facet of the bead crystal was polished to a mirrorlike finish with a 0.25 μm diamond paste. For EC-STM (Nanoscope III, Digital Instruments, USA) work, however, a (111) facet was used without polishing. Well-ordered and clean Pt(111) electrode surfaces were prepared routinely with annealing in a hydrogen flame, followed by quenching in hydrogen-saturated water.

The EC-STM experiments were performed with a homemade EC-STM cell. The W tips (0.25 mm diameter, Aldrich) were made by electrochemical etching in 1 M KOH solution with 15 V ac and coated with melted polyethylene. The direction of the Pt(111) surface was confirmed by observing the Pt atoms along with the Ru and Os deposits.

The Ru and Os solutions were obtained by dissolving $RuCl_3 \cdot xH_2O$ (Aldrich, 99.98%) and $OsCl_3$ (Aldrich, 99.9%) in 0.1 M $HClO_4$ (Merck, Suprapur). The concentrations of $RuCl_3$ and $OsCl_3$ were 0.5 and 2 mM, respectively. Both of the solutions were aged 2 weeks to form stable aqua complexes of Ru and Os ions.[19,24] The 2 mM Os solution was diluted 20 times before deposition. The spontaneous deposition of Ru and Os was performed with a contact of a well-ordered Pt(111) electrode, confirmed with voltammetry, with the Ru or Os ion containing solutions for a proper amount of time to control the coverage of metal deposits.

The potentials of Pt(111) electrodes in EC-STM and voltammetric experiments were controlled against a Ag/AgCl reference electrode with an 1.0 M Cl^- solution, and the potentials in this work are reported as measured.

Results and Discussion

Electrochemistry of Ru and Os Deposits. Figure 1 shows the cyclic voltammograms of Ru and Os spontaneously deposited on Pt(111). After inducing spontaneous deposition of Ru by dipping a clean Pt(111) electrode (the thin solid lines in Figure 1) into 0.5 mM $RuCl_3$ + 0.1 M $HClO_4$ solution for 30 s without potential control, the cyclic voltammogram in Figure 1a was obtained in 0.05 M H_2SO_4 solution. During the initial

10.1021/jp062143z CCC: $33.50
Published on Web 06/20/2006

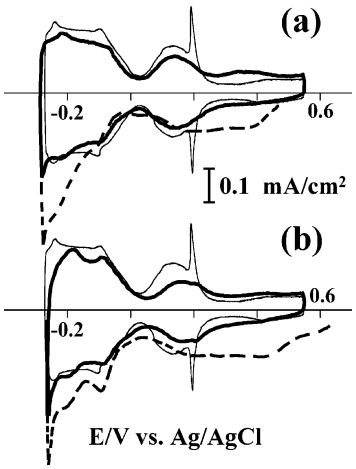

Figure 1. Cyclic voltammograms of Pt(111) covered with spontaneously deposited (a) Ru and (b) Os in 0.05 M H_2SO_4. The deposition of Ru and Os was carried out in 0.5 mM $RuCl_3$ + 0.1 M $HClO_4$ for 0.5 min and 0.1 mM $OsCl_3$ + 0.1 M $HClO_4$ for 2 min, respectively. The solid lines, dashed lines, and thick solid lines stand for the voltammograms of clean Pt(111), initial voltammograms of modified Pt(111), and ultimate voltammograms of modified Pt(111), respectively. Scan rate: 50 mV/s.

cathodic scan from the open-circuit potential (~0.63 V), the reduction currents (dashed line) were observed in two potential regions: −0.25−0 V and 0−0.57 V. In the potential interval of −0.25−0 V, the oxygenated Ru adsorbates (see below) are reduced, whereas in the potential region of 0−0.57 V, a certain Pt oxide, probably formed during handling of the Pt(111) electrode, is reduced. In the next voltammetric cycle, the voltammogram changes immediately to the one presented with the thick solid line. The XPS results revealed that, below 0 V, most of the adsorbed Ru remains as Ru(0), while above 0 V the Ru deposits become RuO_2 and/or RuO_3.[18] On the other hand, the deposition of Os was carried out in 0.1 mM $OsCl_3$ + 0.1 M $HClO_4$ solution for 2 min without potential control. After the electrode was rinsed with water, the cyclic voltammogram in Figure 1b was obtained. The open-circuit potential was measured to be ~0.62 V, where a voltammetric scan was taken in the cathodic direction. The initial voltammogram of Os, displayed with the dashed line, shows two reduction potential regions as well as that of Ru. The reduction current of Os below 0 V, however, decreases gradually in a few subsequent voltammetric cycles, so that the ultimate voltammogram is the one of the thick solid line in Figure 1b. The ex situ XPS and in situ GIF-XAS results[22] verified that the oxidation states of Os deposits depend on the electrode potential: below 0.2 V, the Os deposits are purely metallic, while in the potential region between 0.2 and 0.6 V the portion of Os^{4+} increases as the potential increases.

It is important to keep in mind that, in the pristine layers of Ru and Os, significant amounts of surface oxygen were found by XPS studies.[18,22] These specific observations clearly indicate that the chemical states of the pristine layers of Ru and Os are oxygenated species such as oxides or hydroxides. In the pristine layer of Os, furthermore, there was no XPS signal regarding chlorine despite the presence of chloride ions in the Os-containing solution.[22] The absence of chlorine may be understood in terms of formation of the depositing aqua complexes of Os, not coordinated to chloride, during the solution aging period as described in the Experimental Section. It has been suggested, however, that the chloride in the solutions containing the metal ions may inhibit a continuous growth of the metal deposits, probably by strongly adsorbing near the nanodeposits.

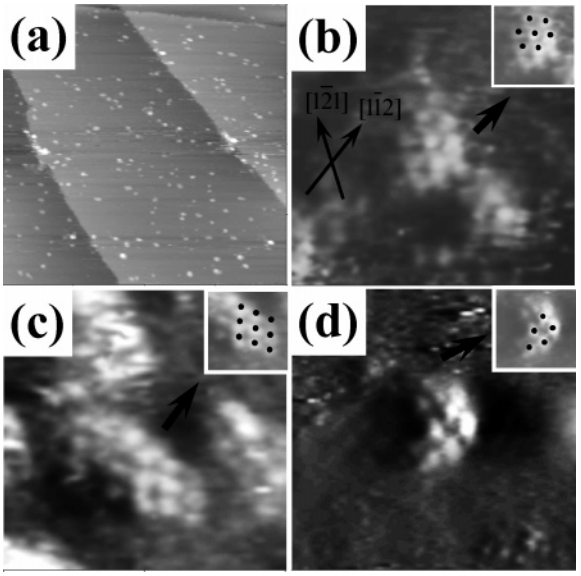

Figure 2. Typical EC-STM images of Ru nanodeposits on Pt(111) in 0.05 M H_2SO_4 solution: (a) large-scale image (100 nm × 100 nm) at open-circuit potential, atomic-scale images (5 nm × 5 nm) at (b) open-circuit potential, (c) reducing potential (0.0 V), and (d) oxidizing potential (0.45 V). Tip bias: (a) −250, (b) 12.6, (c) −123, and (d) −432 mV. Tip current: (a) 0.8, (b) 2.8, (c) 1.2, and (d) 5 nA.

Therefore, the presence of chloride inside the nanodeposits under investigation could be excluded.

Electrochemical STM Images of the Deposits of Ru and Os. Figure 2 shows the typical STM images of the Ru deposits on Pt(111). The deposition of Ru was conducted in the same manner as described in the previous section, and a large-scale STM image (100 nm × 100 nm) is shown in Figure 2a. The Ru deposits are scattered randomly without any local preference for surface features such as step, and their sizes are distributed in the range of 2−5 nm in diameter as reported previously.[17,23] In addition, the heights of the deposits are exclusively monatomic under the specific deposition condition. The coverage of Ru, defined as the ratio of the area of the Ru deposits to that of the whole image (1×10^4 nm^2), is ~0.05 (a single contact for more than 3 min with the Ru^{3+}-containing solution guarantees the Ru deposits whose height and coverage are monatomic and more than 0.2, respectively.). The particular low coverage was purposefully for imaging at an atomic scale, because it was practically impossible to observe the arrangements of Ru atoms in the small nanosized islands on an atomically rough Pt(111) surface of a high Ru coverage above 0.1. Figure 2b was obtained at open-circuit potential, i.e., ~0.63 V, where the Ru deposits are known to be oxygenated.[18] In a Ru deposit of ~2 nm in diameter, it is clear that the spots are arranged in a hexagonal symmetry (see the inset of Figure 2b). The periodicities of the spots in the [1$\bar{1}$2] and [1$\bar{2}$1] directions are 0.46 ± 0.02 nm and 0.47 ± 0.01 nm, respectively. Taking it into account that one Pt−Pt distance (thereafter referred as *a*) is 0.277 nm, the measured distances between the spots indicate that the atoms in the pristine Ru deposits are arrayed in a $(\sqrt{3}\times\sqrt{3})R30°$ pattern. Upon reduction at 0.0 V, however, the unit cell in the Ru deposit is changed to a uniaxially incommensurate $(\sqrt{3}\times\sqrt{2})$-$R30°$ arrangement. Specifically, as shown in Figure 2c, the spot frequency in the [1$\bar{2}$1] direction reduces to 0.39 ± 0.02 nm, i.e., $\sqrt{2}a$, while that in the [1$\bar{1}$2] direction remains constant at 0.48 ± 0.02 nm, i.e., $\sqrt{3}a$. Indeed, the hexagon in the inset of Figure 2c is distorted slightly due to the decrease in the spot−spot distance in the [1$\bar{2}$1] direction. Because the local coverage of the deposits is not modified significantly, the spots in Figure

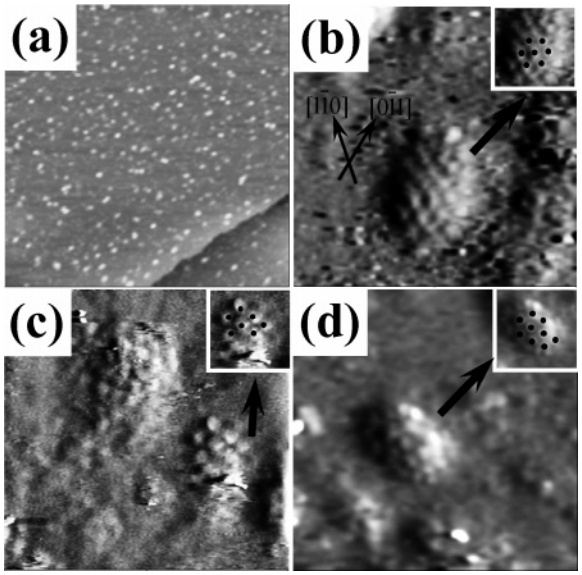

Figure 3. Typical EC-STM images of Os nanodeposits on Pt(111) in 0.05 M H_2SO_4 solution: (a) large-scale image (100 nm × 100 nm) at open-circuit potential, atomic-scale images (5 nm × 5 nm) at (b) open-circuit potential, (c) reducing potential (0.0 V), and (d) oxidizing potential (0.45 V). Tip bias: (a) −245.4, (b) −245.4, (c) 177, and (d) −284 mV. Tip current: (a) 2.0, (b) 2.5, (c) 4.3, and (d) 3.74 nA.

2b,c are assignable to Ru; thus, the oxygen ions, not visible under the employed imaging condition, would be imbedded among the Ru atoms at open-circuit potential. Then, the change of the Ru unit cell during reduction supports that the electrochemical removal of the oxygen ions in the pristine Ru deposits may lead to the more compact Ru array, or the uniaxially incommensurate $(\sqrt{3}\times\sqrt{2})R30°$ lattice. The rearrangement of Ru after reduction is probably due to the instability of the metallic Ru arrayed in the $(\sqrt{3}\times\sqrt{3})R30°$ pattern without oxygen ions. The shrinkage of the pristine Ru deposits on Pt(111), not in an atomic scale, was reported by Wieckowski's group,[25] and similar rearrangements of elemental Te[26] and Sb[27] after reduction of their oxygenated layers on Pt(111) were demonstrated by our group. Reoxidation of the Ru deposits at 0.45 V, on the other hand, does not induce any further change in the arrangement of Ru, as shown in Figure 2d. In other words, the unit cell of Ru in the reoxidized Ru deposit is a uniaxially incommensurate $(\sqrt{3}\times\sqrt{2})R30°$ structure as well as that of the reduced deposits. Because the oxygen ions are not observable in this work, it is not clearly understood how the oxygen ions react with the elemental Ru islands. It is obvious, however, that the reoxidized Ru deposits are not the same as their pristine ones. Once the pristine layer of Ru on Pt(111) is reduced, therefore, the uniaxially incommensurate $(\sqrt{3}\times\sqrt{2})R30°$ structure is maintained regardless of electrode potential unless stripped.

Figure 3 shows typical STM images of Os on Pt(111). The adsorption of Os was conducted in a solution of low Os concentration, i.e., 0.1 mM $OsCl_3$. As shown in Figure 3a, the nanodeposits of Os are distributed homogeneously, and the coverage of Os, defined as above, is 0.14, low enough to image at the atomic level. Despite the low coverage, however, Os nanoislands of multilayers were found as well as those of monatomic height, which is not the case for Ru. This observation is coherent with the adsorptive behavior of Os reported previously by Wieckowski.[19] Parts b, c , and d of Figure 3 are typical STM atomic images of Os nanodeposits of monatomic height obtained at open-circuit potential (∼0.62 V), 0.0 V, and 0.45 V, respectively. In Figure 3b, the spot periodicities observed

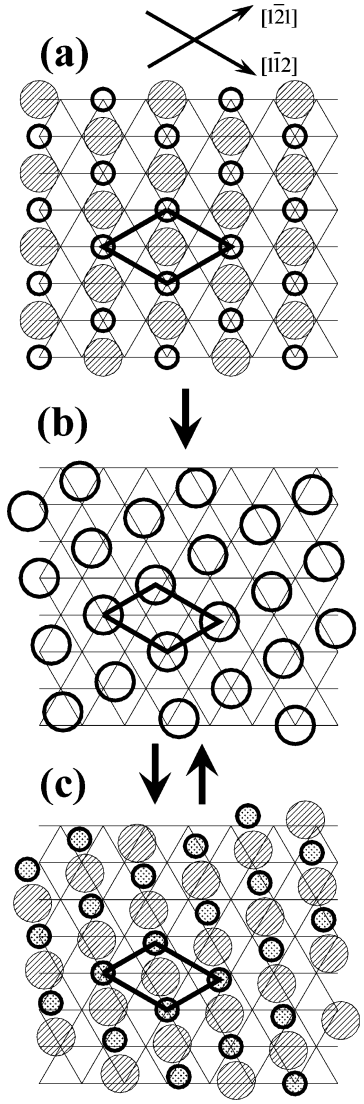

Figure 4. Schematic for the proposed atomic arrangements inside Ru nanoislands spontaneously deposited on Pt(111): (a) $(\sqrt{3}\times\sqrt{3})R30°$-$RuO^+$ at open-circuit potential, (b) uniaxially incommensurate $(\sqrt{3}\times\sqrt{2})$-$R30°$-Ru at 0.0 V, and (c) uniaxially incommensurate $(\sqrt{3}\times\sqrt{2})R30°$-$RuO^{x+}$ ($x > 3$) at 0.45 V. The hexagonal grid represents the basal plane of Pt(111), and the hatched circles stand for O^{2-} ions. The small and large open circles in (a) and (b) are Ru^{3+} ions and elemental Ru atoms, respectively. The small circles filled with dots in (c) are Ru ions whose oxidation numbers are more than 3. The sizes of all the atoms or ions are scaled to one Pt−Pt distance (0.277 nm).

on the pristine layer of Os are 0.37 ± 0.03 nm and 0.38 ± 0.03 nm in the [0$\bar{1}$1] and [1$\bar{1}$0] directions, respectively. When the pristine Os islands are reduced at 0.0 V, the frequencies of the spots do not change at all (Figure 3c). Therefore, it is concluded that the Os atoms in the deposits spontaneously deposited on Pt(111) are arranged in an incommensurate $(\sqrt{2}\times\sqrt{2})$ pattern. Considering that an XPS and GIF-XAS study on Os[22] evidenced the presence of oxygen among the pristine Os deposits, the reductive stripping of the oxygen ions in the pristine Os layer does not induce any shrink of the metallic Os islands, which is contrasting with Ru on Pt(111). In addition, reoxidation of the Os layer does not alter the spot periodicity, either (Figure 3d). Therefore, the incommensurate $(\sqrt{2}\times\sqrt{2})$ adlattice of Os is concluded to be persistent at any potential before oxidative stripping.

It is worthwhile to address the reproducibility of the atomic arrangements inside the nanoislands, and thereby the precisions

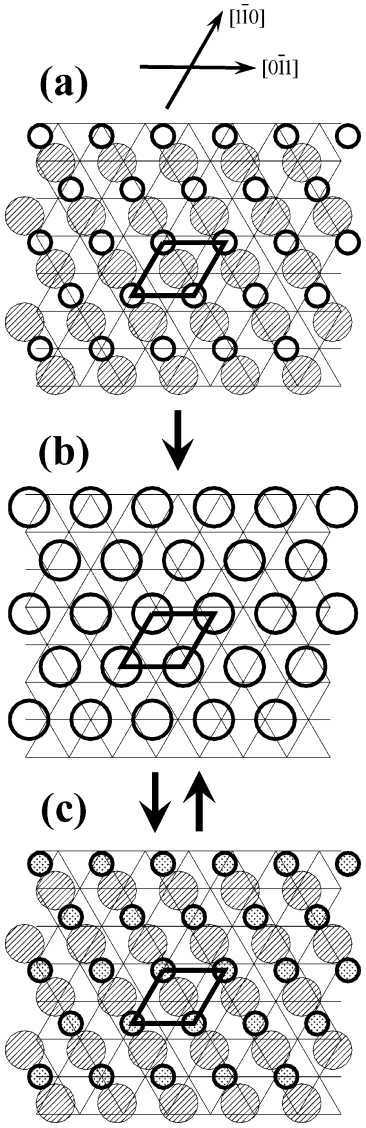

Figure 5. Schematic for the proposed atomic arrangements inside Os nanoislands spontaneously deposited on Pt(111): (a) incommensurate ($\sqrt{2}\times\sqrt{2}$)-OsO^+ at open-circuit potential, (b) incommensurate ($\sqrt{2}\times\sqrt{2}$)-Os at 0.0 V, and (c) incommensurate ($\sqrt{2}\times\sqrt{2}$)-OsO^{2+} at 0.45 V. The hexagonal grid represents the basal plane of Pt(111), and the hatched circles stand for O^{2-} ions. The small and large open circles in (a) and (b) are Os^{3+} ions and elemental Os atoms, respectively. The small circles filled with dots in (c) are Os^{4+} ions. The sizes of all the atoms or ions are scaled to one Pt−Pt distance (0.277 nm).

of the numerical values presented as above. Since the sizes of the islands are several atomic rows, one may be doubtful concerning the reproducibility of the assigned adstructures. To keep the reported values statistically meaningful, several replica experiments, at least more than 5, were carried out, and then the reported values were obtained after treating statistically the measured spot frequencies of the islands observed in the different replica experiments. Therefore, we believe that the precisions of the lattice parameters reported in this work are good enough.

The schematics in Figure 4 are proposed for the observed adstructures of Ru. In Figure 4a, Ru^{3+} ions (0.082 nm radius[28]) are arrayed in a ($\sqrt{3}\times\sqrt{3}$)*R*30° pattern, and O^{2-} ions (0.124 nm radius[28]) are placed at the center of the unit cell, assuming that the oxidation number of Ru does not change during deposition. Thus, two-dimensional oxide nanoislands of ($\sqrt{3}\times\sqrt{3}$)*R*30°-RuO^+ are produced, whose positive charge may be compensated by the adsorption of bisulfate anions.[26,27] The reductive stripping of the oxygen in the oxide layer would lead to an unstable array of elemental Ru in the ($\sqrt{3}\times\sqrt{3}$)*R*30° pattern, so that a compression of the Ru atoms in the [1$\bar{2}$1] direction transforms the unstable structure to the uniaxially incommensurate ($\sqrt{3}\times\sqrt{2}$)*R*30°-Ru structure (Figure 4b). During the reoxidation, the oxygen ions from water molecules would be inserted into the centers of the uniaxially incommensurate ($\sqrt{3}\times\sqrt{2}$)*R*30° unit cells as shown in Figure 4c. Since the oxidation number of the Ru ions in the deposits has been verified to be higher than 3,[18] the vacancies inside the ($\sqrt{3}\times\sqrt{2}$)*R*30° unit cell would be spacious enough to place one O^{2-} ion.

Figure 5 shows schematics of Os adstructures on Pt(111). As shown in Figure 5a, the Os^{3+} ions are located in an incommensurate ($\sqrt{2}\times\sqrt{2}$) pattern, and the O^{2-} ions are positioned at the centers of the unit cells. The length of the shorter diagonal in the ($\sqrt{2}\times\sqrt{2}$) unit cell, $\sqrt{2}a = 0.39$ nm, is just enough to accommodate one Os^{3+} ion and one O^{2-} ion (since the radius of Os^{3+} ion was not found in any literature, the radius is assumed to be similar to that of Ru^{3+} ion, 0.082 nm). Thus, it is clear that the pristine deposits of the incommensurate ($\sqrt{2}\times\sqrt{2}$)-OsO^+ form more compact adlayers than those of Ru, assuming again that the oxidation number of Os does not change during deposition. Such a compactness of the pristine Os deposits may imply that the interaction among the Os adsorbates within a deposit is stronger than the interaction between the adsorbates and the substrate; in turn, multilayer Os deposits may be formed more easily than Ru deposits, as confirmed previously by Wieckowski.[19] The reduction of the Os deposits, i.e., removal of oxygen ions from the deposits, does not induce any modification of the adstructure. The reason for the absence of structural change may be because the metallic Os atoms are already close enough to not need any further rearrangement. The incommensurate ($\sqrt{2}\times\sqrt{2}$) array is maintained even after reoxidation of the metallic Os to Os^{4+} ions.[22]

Summary

The EC-STM atomic images of Ru and Os deposited spontaneously on Pt(111) are presented. In the pristine layer of Ru, the Ru ions are arrayed in a ($\sqrt{3}\times\sqrt{3}$)*R*30°-RuO^+ pattern. The reduction of the Ru layer, however, induces a transformation of the adstructure to a uniaxially incommensurate ($\sqrt{3}\times\sqrt{2}$)-*R*30°-Ru structure, which is not changed even after reoxidation of the metallic Ru layer. In the Os deposits, on the other hand, an incommensurate ($\sqrt{2}\times\sqrt{2}$) adlattice is persistent, regardless of electrochemical treatments. The schematics of the Ru and Os superstructures are suggested and discussed in terms of removal and insertion of oxygen ions depending on electrode potential.

Acknowledgment. The authors appreciate the permission from the Central Research Facility, Chungnam National University, Korea, for use of the STM instrument. This work was supported by the Korea Research Foundation Grant funded by the Korean Government (MOEHRD) (R05-2004-000-10247-0).

References and Notes

(1) Watanabe, M.; Motoo, S. *J. Electroanal. Chem.* **1975**, *60*, 267.

(2) Iwasita, T.; Nart, F. C.; Vielstich, W. *Ber. Bunsen-Ges. Phys. Chem.* **1990**, *94*, 1030.

(3) Gasteiger, H. A.; Markovic, N.; Ross, P. N., Jr.; Cairns, E. J. *J. Electrochem. Soc.* **1994**, *141*, 1795.

(4) Markovic, N. M.; Gasteiger, H. A.; Ross, P. N., Jr.; Jiang, X.; Villegas, I.; Weaver, M. J. *Electrochim. Acta* **1995**, *40*, 91.
(5) Chrzanowski, W.; Kim, H.; Wieckowski, A. *Catal. Lett.* **1998**, *50*, 69.
(6) Iwasita, T.; Hoster, H.; John-Anacker, A.; Lin, W. F.; Vielstich, W. *Langmuir* **2000**, *16*, 522.
(7) Hoster, H.; Iwasita, T.; Baumgartner, H.; Vielstich, W. *J. Electrochem. Soc.* **2001**, *148*, A496.
(8) Hoster, H.; Iwasita, T.; Baumgartner, H.; Vielstich, W. *Phys. Chem. Chem. Phys.* **2001**, *3*, 337.
(9) Babu, P. K.; Tong, Y. Y.; Kim, H. S.; Wieckowski, A. *J. Electroanal. Chem.* **2002**, *524*−*525*, 157.
(10) Tong, Y.; Kim, H. S.; Babu, P. K.; Waszczuk, P.; Wieckowski, A.; Oldfield, E. *J. Am. Chem. Soc.* **2002**, *124*, 468.
(11) Gurau, B.; Viswanathan, R.; Liu, R.; Lafrenz, T. J.; Ley, K. L.; Smotkin, E. S.; Reddington, E.; Sapienza, A.; Chan, B. C.; Mallouk, T. E.; Sarangapani, S. *J. Phys. Chem. B* **1998**, *102*, 9997.
(12) Reddington, E.; Sapienza, A.; Gurau, B.; Viswanathan, R.; Sarangapani, S.; Smotkin, E. S.; Mallouk, T. E. *Science* **1998**, *280*, 1735.
(13) Kabbabi, A.; Faure, R.; Durand, R.; Beden, B.; Hahn, F.; Leger, J. M.; Lamy, C. *J. Electroanal. Chem.* **1998**, *444*, 41.
(14) Frelink, T.; Visscher, W.; van Veen, J. A. R. *Surf. Sci.* **1995**, *335*, 353.
(15) Frelink, T.; Visscher, W.; van Veen, J. A. R. *Langmuir* **1996**, *12*, 3702.
(16) Abd El Meguid, E. A.; Berenz, P.; Baltruschat, H. *J. Electroanal. Chem.* **1999**, *467*, 50.
(17) Crown, A.; Wieckowski, A. *Phys. Chem. Chem. Phys.* **2001**, *3*, 3290.
(18) Kim, H.; Rabelo de Moraes, I.; Tremiliosi-Filho, G.; Haasch, R.; Wieckowski, A. *Surf. Sci.* **2001**, *474*, L203.
(19) Strbac, S.; Johnston, C. M.; Lu, G. Q.; Crown, A.; Wieckowski, A. *Surf. Sci.* **2004**, *573*, 80.
(20) Chrzanowski, W.; Kim, H.; Tremiliosi-Filho, G.; Wieckowski, A.; Grzybowska, B.; Kulesza, P. *J. New Mater. Electrochem. Syst.* **1998**, *1*, 31.
(21) Lu, C.; Masel, R. I. *J. Phys. Chem. B* **2001**, *105*, 9793.
(22) Rhee, C. K.; Wakisaka, M.; Tolmachev, Y. V.; Johnston, C. M.; Haasch, R.; Attenkofer, K.; Lu, G. Q.; You, H.; Wieckowski, A. *J. Electroanal. Chem.* **2003**, *554*−*555*, 367.
(23) Crown, A.; Moraes, I. R.; Wieckowski, A. *J. Electroanal. Chem.* **2001**, *500*, 333.
(24) Chrzanowski, W.; Wieckowski, A. *Langmuir* **1997**, *13*, 5974.
(25) Crown, A.; Kim, H.; Lu, G. Q.; de Moraes, I. R.; Rice, C.; Wieckowski, A. *J. New Mater. Electrochem. Syst.* **2000**, *3*, 275.
(26) Rhee, C. K.; Jung, C.; Ku, B. *J. Solid State Electrochem.* **2005**, *9*, 247.
(27) Zhao, J.; Jung, C.; Rhee, C. K. *J. Phys. Chem. B* **2006**, in press.
(28) Shannon, R. D. *Acta Crystallogr., Sect. A* **1976**, *A32*, 751.